

Unraveling Quantum Annealers using Classical Hardness

Victor Martin-Mayor

*Departamento de Física Teórica I, Universidad Complutense, 28040 Madrid, Spain and
Instituto de Biocomputación y Física de Sistemas Complejos (BIFI), Zaragoza, Spain*

Itay Hen

Information Sciences Institute, University of Southern California, Marina del Rey, California 90292, USA

(Dated: March 1, 2022)

Recent advances in quantum technology have led to the development and manufacturing of experimental programmable quantum annealing optimizers that contain hundreds of quantum bits. These optimizers, named ‘D-Wave’ chips, promise to solve practical optimization problems potentially faster than conventional ‘classical’ computers. Attempts to quantify the quantum nature of these chips have been met with both excitement and skepticism but have also brought up numerous fundamental questions pertaining to the distinguishability of quantum annealers from their classical thermal counterparts. Here, we propose a general method aimed at answering these, and apply it to experimentally study the D-Wave chip. Inspired by spin-glass theory, we generate optimization problems with a wide spectrum of ‘classical hardness’, which we also define. By investigating the chip’s response to classical hardness, we surprisingly find that the chip’s performance scales unfavorably as compared to several analogous classical algorithms. We detect, quantify and discuss purely classical effects that possibly mask the quantum behavior of the chip.

I. INTRODUCTION

Interest in quantum computing originates in the potential of quantum computers to solve certain computational problems much faster than is possible classically, due to the unique properties of Quantum Mechanics [1, 2]. The implications of having at our disposal reliable quantum computing devices are obviously tremendous. The actual implementation of quantum computing devices is however hindered by many challenging difficulties, the most prominent being the control or removal of quantum decoherence [3]. In the past few years, quantum technology has matured to the point where limited, task-specific, non-universal quantum devices such as quantum communication systems, quantum random number generators and quantum simulators, are being built, possessing capabilities that exceed those of corresponding classical computers.

Recently, a programmable quantum annealing machine, known as the D-Wave chip [4], has been built whose goal is to minimize the cost functions of classically-hard optimization problems presumably by adiabatically quenching quantum fluctuations. If found useful, the chip could be regarded as a prototype for general-purpose quantum optimizers, due to the broad range of hard theoretical and practical problems that may be encoded on it.

The capabilities, performance and underlying physical mechanism driving the D-Wave chip have generated fair amounts of curiosity, interest, debate and controversy within the Quantum Computing community and beyond, as to the true nature of the device and its potential to exhibit clear “quantum signatures”. While some studies have concluded that the behavior of the chip is consistent with quantum open-system Lindbladian dynamics [5] or indirectly observed entanglement [6], other studies con-

testing these [7, 8] pointed to the existence of simple, purely classical, models capable of exhibiting the main characteristics of the chip.

Nonetheless, the debate around the quantum nature of the chip has raised several fundamental questions pertaining to the manner in which quantum devices should be characterized in the absence of clear practical “signatures” such as (quantum) speedups [9, 10]. Since quantum annealers are meant to utilize an altogether different mechanism for solving optimization problems than traditional classical devices, methods for quantifying this difference are expected to serve as important theoretical tools while also having vast practical implications.

Here, we propose a method that partly solves the above question by providing a technique to characterize, or measure, the “classicality” of quantum annealers. This is done by studying the algorithmic performance of quantum annealers on sets of optimization problems possessing quantifiable, varying degrees of “thermal” or “classical” hardness, which we also define for this purpose. To illustrate the potential of the proposed technique, we apply it to the experimental quantum annealing optimizer, the D-Wave Two (DW2) chip.

We observe several distinctive phenomena that reveal a strong correlation between the performance of the chip and classical hardness: i) The D-Wave chip’s typical time-to-solution (t_s) as a function of classical hardness scales differently, in fact worse, than that of thermal classical algorithms. Specifically, we find that the chip does very poorly on problem instances exhibiting a phenomenon known as “temperature chaos”. ii) Fluctuations in success probability between programming cycles become larger with increasing hardness, pointing to the fact that encoding errors become more pronounced and destructive with increasing hardness. iii) The success probabilities obtained from harder instances are affected

more than easy instances by changes in the duration of the anneals.

Analyzing the above findings, we identify two major probable causes for the chip’s observed “sub-classical” performance, namely i) that its temperature may not be low enough, and ii) that encoding errors become more pronounced with increasing hardness. We further offer experiments and simulations designed to detect and subsequently rectify these so as to enhance the chip’s capabilities.

II. CLASSICAL HARDNESS, TEMPERATURE CHAOS AND PARALLEL TEMPERING

In order to study the manner in which the performance of quantum annealers correlates with ‘classical hardness’, it is important to first accurately establish the meaning of *classical hardness*. For that purpose, we refer to spin-glass theory [11], which deals with *spin glasses*—disordered, frustrated spin systems that may be viewed as prototypical classically-hard (also called NP-hard) optimization problems, that are so challenging that specialized hardware has been built to simulate them [12–14].

Currently, the (classical) method of choice to study general spin-glass problems is Parallel Tempering (PT, also known as ‘exchange Monte Carlo’) [15, 16]. PT is a refinement of the celebrated yet somewhat outdated Simulated Annealing algorithm [17], that finds optimal assignments (i.e., the ground-state configurations) of given discrete-variable cost functions. It is therefore only natural to make use of the performance of PT to characterize and quantify classical hardness.

In PT simulations, one considers N_T copies of an N -spin system at temperatures $T_1 < T_2 < \dots < T_{N_T}$, where each copy undergoes Metropolis spin-flip updates independently of other copies. In addition, copies with neighboring temperatures regularly attempt to swap their temperatures with probabilities that satisfy detailed balance [18]. In this way, each copy performs a temperature random-walk (see inset of Fig 1). At high temperatures, free-energy barriers are easily overcome, allowing for a global exploration of configuration space. At lower temperatures on the other hand, the local minima are explored in more detail. A ‘healthy’ PT simulation requires an unimpeded temperature flow: The total length of the simulation should be longer than the temperature ‘mixing time’ τ [19, 20]. The time τ may be thought of as the average time it takes each copy to fully traverse the temperature mesh, indicating equilibration of the simulation. Therefore, instances with large τ are harder to equilibrate, which motivates our definition of the mixing time τ as the *classical hardness* of a given instance.

Despite the popularity of PT, it has also become apparent that not all the spin-glass problems can be efficiently solved by the algorithm [20, 21]. The reason is a phenomenon that has become known as *Temperature Chaos* (TC). TC [21–36] consists of a sequence of first-order

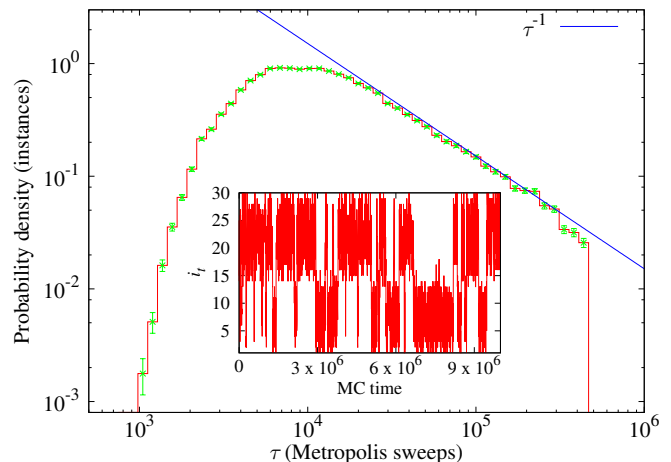


FIG. 1. **Probability distribution of mixing times τ over random $J = \pm 1$ ‘Chimera’ instances as extracted from the PT random-walk on the temperature grid.** The solid line is a linear fit to the tail of the distribution, implying the existence of rare instances with very long mixing times (note that a τ^{-1} tail is not strictly integrable, hence this specific power law decay should only be regarded as a finite-size approximation). **Inset:** Example of a temperature random walk for an instance with $\tau \approx 1.8 \times 10^5$. Considering one of $N_T = 30$ copies of the system, at any given Monte Carlo time t , the copy’s temperature is T_{it} . In this example, the replica has visited each temperature several times, pointing to the fact that the simulation time is longer than the mixing time τ .

phase transitions that a given spin-glass instance experiences upon lowering its temperature, whereby the dominant configurations minimizing the free energy above the critical temperatures are vastly different than those below them (Fig. 2 depicts such a phase that is ‘rounded’ due to the finite size of the system). A given instance may experience zero, one or more transitions at random temperatures, making the study of TC excruciatingly difficult [21, 34–36]. Such TC transitions hinder the PT temperature flow, significantly prolonging the mixing time τ . In practice [21], it is found that for small systems the large majority of the instances do not suffer any TC transitions and are ‘easy’ (i.e., they are characterized by short mixing times). However, for a minor fraction of them, τ turns out to be inordinately large. Moreover, the larger the system is, the larger the fraction of long- τ samples becomes. In the large N limit, these are the short- τ samples that become exponentially rare in N [21, 32]. This provides further motivation for studying TC instances of optimization problems on moderately small experimental devices (even if they are rare).

III. TEMPERATURE CHAOS AND QUANTUM ANNEALERS

With the advent of quantum annealers, which presumably offer non-thermal mechanisms for finding ground

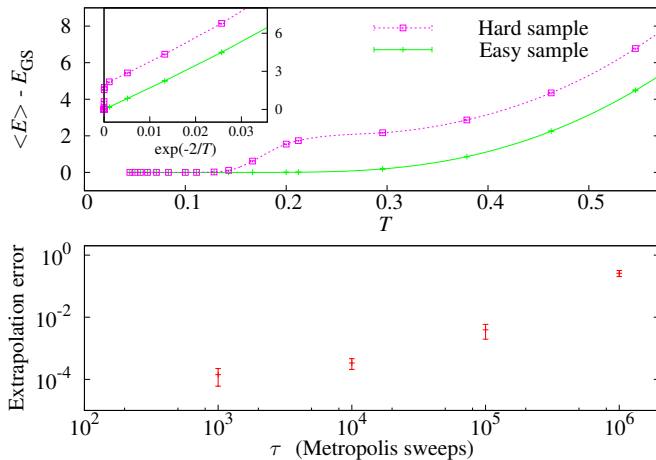


FIG. 2. **Top: Energy above the ground-state energy as a function of temperature for two randomly chosen instances.** The mixing times of the two instances are $\tau \approx 10^3$ (“easy”) and $\tau \approx 10^6$ (“hard”). Unlike the easy sample, the hard sample exhibits “temperature chaos”: Upon lowering the temperature, the energy decreases at first in a gradual manner, however at $T \approx 0.2$ there is a sudden drop indicating that a different set of minimizing configurations has been visited. **Inset:** Main panel’s data vs. $\exp(-\Delta/T)$ (where $\Delta = 2$ is the excitation gap). A linear behavior is expected if the system can be described as a gas of non-interacting excitations over a local energy minimum. For the easy sample, this local minimum is a ground state. On the other hand, for instances displaying TC above their chaos temperature, the local-minimum energy is higher than the ground-state’s. **Bottom: τ -dependence of the median systematic error (for each τ -generation) of a $T \rightarrow 0$ extrapolation of the total energy.** For each instance, we extrapolated the $T = 0.2, 0.3$ data linearly in $\exp(-\Delta/T)$ and compared this extrapolation with the actual ground-state energy.

states, it has become only natural to ask whether quantum annealers can be used to solve ‘TC-ridden’ optimization problems faster than classical techniques such as PT. In this context, the question of how the performance of quantum annealers depends on the ‘classical hardness’ becomes of fundamental interest: If indeed quantum annealers exploit quantum phenomena such as tunneling to traverse energy barriers, one may hope that they will not be as sensitive to the thermal hardness (as defined above) of the optimization problems they solve. As we shall see next, having a practical definition for classical hardness allows us to address the above questions directly.

To illustrate this, in what follows we apply the ideas introduced above to the DW2 quantum annealing optimizer in order to infer its degree of ‘classicality’. We accomplish this by first generating an ensemble of instances that are directly embeddable on the DW2 ‘Chimera’ architecture [the reader is referred to Appendix C for a detailed description of the Chimera lattice and the D-wave chip and its properties]. The chip on which we perform our study is an array of 512 superconducting flux qubits of which only 476 are functional, operating

at a temperature of ~ 15 mK. The DW2 chip is designed to solve a very specific type of problems, namely, Ising-type optimization problems, by adiabatically transitioning the system Hamiltonian from an initial transverse-field Hamiltonian to a final classical programmable cost function of a typical spin glass. The latter is given by the Ising Hamiltonian:

$$H_{\text{Ising}} = \sum_{\langle ij \rangle} J_{ij} s_i s_j + \sum_i h_i s_i. \quad (1)$$

The Ising spins, $s_i = \pm 1$ are the variables to be optimized over, and the sets $\{J_{ij}\}$ and $\{h_i\}$ are programmable parameters of the cost function. Here, $\langle ij \rangle$ denotes a sum over all the active edges of the Chimera graph. For simplicity, we conduct our study on randomly-generated problem instances with $h_i = 0$ and random, equiprobable $J_{ij} = \pm J$ couplings (in our energy units $J = 1$).

Initially, it is not clear whether the task of finding thermally-hard instances on the Chimera is feasible. While on the one hand TC has been observed in spin-glasses on the square lattice [37], which has the same spatial dimension, $D = 2$, as the Chimera [38], it has also been found that typical Chimera-embeddable instances are easy to solve [9, 10, 38]. As discussed above, system size plays a significant role in this context, as an $N \sim 512$ -spin Chimera may simply be too small to have instances exhibiting TC.¹ Taking a brute-force approach to resolve this issue, we generated $\sim 80,000$ random problem instances (each characterized by a different set of $\{J_{ij}\}$), analyzing each one by running them on a state-of-the-art PT algorithm until equilibration was reached (Appendix B). This allowed for the calculation of the instances’ classical hardness, namely their temperature mixing times τ (for more details, see Appendix A, below). The resulting distribution of τ over the instances is shown in Fig. 1. While most instances equilibrate rather quickly (after some 10^4 MC steps), we find that the distribution has a ‘tail’ of hard samples with $\tau > 10^6$ revealing that hard instances, although rare, do exist (we estimate that 2 samples in 10^4 have $\tau > 10^7$).

To study the DW2 chip, we grouped together instances with similar classical hardness, i.e., similar mixing times, $10^k \leq \tau < 3 \cdot 10^k$ for $k = 3, 4, 5, 6$ and 7. For each such ‘generation’ of τ , we randomly picked 100 representative instances for running on the chip (only 14 instances with $k = 7$ were found). As a convergence test of PT on the selected instances, we verified that the ground-state energies reached by PT are the true ones by means of an exact solver.

At the purely classical level, we found, as anticipated [21], that classically hard instances differ from easy instances from a thermodynamic point of view as well.

¹ For instance, on the square lattice one needs to reach $N \sim 512^2 \approx 2.5 \times 10^5$ spins for TC to be the rule rather than the exception [37].

Specifically, large τ instances were found to exhibit sharp changes in the average energy at random critical temperatures, consistently with the occurrence of TC (see Fig. 2). For such instances, the true ground states are present during the simulations only below the TC critical temperatures. As the inset shows, the larger τ is, the lower these critical temperatures typically are. Furthermore, classically-hard instances were found to differ from easier ones in terms of their energy landscape: While for easy instances minimally-excited states typically reside only a few spin flips away from ground state configurations, for classically hard instances, this is not the case (see Appendix B).

IV. CLASSICALITY OF THE “D-WAVE TWO” CHIP

Having sorted and analyzed the randomly-generated instances, we turned to experimentally test the performance of the D-Wave chip on these (for details see Appendix A and C 4). Our experiments consisted of programming the chip to solve each of the 414 instances over a dense mesh of annealing times in the available range of $t_a \in [20\mu s, 20ms]$. The number of attempts, or anneals, that each instance was run for each choice of t_a ranged between 10^5 and 10^8 . By calculating the success probability of the annealer for each instance and annealing time, a typical time-to-solution t_s was obtained for each hardness-group, or ‘ τ -generation’ (see Appendix A). Interestingly, we found that for easy samples ($\tau = 10^3$) the success probability depends only marginally on t_a , pointing to the annealer reaching its asymptotic performance on these. As instances become harder, the sensitivity of success probability to t_a increases significantly. Nonetheless, for all hardness groups, the typical t_s is found to be shortest at the minimally-allowed annealing time of $t_a = 20\mu s$ (see Appendix C 4 for a more detailed discussion).

The main results of our investigation are summarized in Fig. 3 depicting the typical time to solution t_s of the DW2 chip (averaged over instances of same hardness groups, see Appendix A) as a function of classical hardness, or ‘ τ -generation’. As is clear from the figure, the performance of the chip was found to correlate strongly with the ‘thermal hardness’ parameter, indicating the significant role thermal hardness plays in the annealing process. Interestingly, the chip’s response was found to be affected by thermal hardness even more than PT, i.e., more strongly than the classical thermal response: While for PT the time-to-solution scales as $t_s \sim \tau$, the scaling of the D-Wave chip was found to scale as $t_s^{DW2} \sim \tau^{\alpha_{DW2}}$, with $\alpha_{DW2} \approx 1.73$. This scaling is rather surprising given that for quantum annealers to perform better than classical ones, one would expect these to be less susceptible to thermal hardness, not more. Nonetheless, it is clear that the notion of classical hardness is very relevant to the D-wave chip.

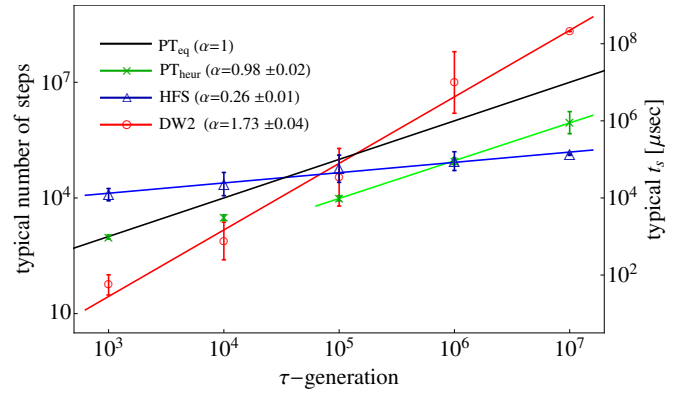


FIG. 3. **Dependence of typical time to solution t_s of the examined optimization algorithms on mixing time τ , the classical hardness parameter.** Classical thermal algorithms scale linearly with τ . Here, PT_{eq} denotes time to equilibration which by definition scales linearly with τ , and PT_{heur} denotes PT functioning as a heuristic solver in which case the time to solution is the number of Monte-Carlo steps to first encounter of a minimizing configuration. The t_s of the classical non-thermal HFS algorithm (measured in μs) scales as $\tau^{\alpha_{HFS}}$, with $\alpha_{HFS} \approx 0.3$. The t_s for the DW2 chip (measured in μs) scales as $\tau^{\alpha_{DW2}}$ with $\alpha_{DW2} \approx 1.73$ (we note the missing error bars on the 10^7 DW2 data point, which is a result of insufficient statistics).

To complete the picture, we have also tested our instances on the Hamze-de Freitas-Selby (HFS) algorithm [39, 40], which is the fastest classical algorithm to date for Chimera-type instances. Even though the HFS algorithm is a ‘non-thermal’ algorithm (i.e., it does not make use of a temperature parameter), we have found the concept of classical hardness to be very relevant here as well. For the HFS algorithm, we find a scaling of $t_s^{HFS} \sim \tau^{\alpha_{HFS}}$ with $\alpha_{HFS} \approx 0.3$, implying that the algorithm is significantly less susceptible to thermal hardness than PT.²

V. ANALYSIS OF FINDINGS

The above somewhat less-than-favorable performance of the experimental D-wave chip on thermally-hard problems is not necessarily a manifestation of the intrinsic limitations of quantum annealing, i.e., it does not necessarily imply that the ‘quantum landscape’ of the tested problems is harder to traverse than the classical one (although this may sometimes be the case [41, 42]). A careful analysis of the results suggests in fact at least two different more probable ‘classical’ causes for the chip’s performance.

² It is worth pointing out that the typical runtime for the HFS algorithm on the hardest, $\tau = 10^7$, group problems was found to be $\sim 0.5s$ on an Intel Xeon CPU E5462 @ 2.80GHz, which to our knowledge makes these the hardest known Chimera-type instances to date.

First, as already discussed above and succinctly captured in Fig. 2, temperature is expected to play a key role in DW2 success on instances exhibiting TC. This is because for these, the ground state configurations minimize the free energy only below the lowest critical TC temperature. Even though the working temperature of the DW2 chip is rather low, namely $\sim 15\text{mK}$, the crucial figure of merit is the ratio of coupling to temperature T/J [recall Eq. (1)]. Although the nominal value for the chip is $T/J \approx 0.1$, any inhomogeneity of the temperature across the chip may render the ratio higher [43], possibly driving it above typical TC critical temperatures.³

Another possible cause for the above scaling may be due to the analog nature of the chip. The programming of the coupling parameters J_{ij} and magnetic fields h_i is prone to statistical and systematic errors (also referred to as intrinsic control errors, or ICE). The couplings actually encoded in DW2 are $J_{ij} = \pm J + R$, where $R \sim \mathcal{N}(0, \delta J)$ is a random error ($\delta J \approx 0.05J$, according to the chip’s manufacturer). Unfortunately, even tiny changes in coupling values are known to potentially change the ground-state configurations of spin glasses in a dramatic manner [35, 45–47]. We refer to this effect as ‘coupling chaos’ (or J -chaos, for short). For an N -bit system, J -chaos seems to become significant for $\delta J_{\text{crit}} \sim |J|/N^a$. Empirically [35, 47] $a \approx 1/D$, D being the spatial dimensionality of the system. Note, however, that these estimates refer only to typical instances and small N whereas the assessment of the effects of J -chaos on thermally-hard instances remains an important open problem for classical spin glasses.

Here, we empirically quantify the effects of J -chaos by taking advantage of the many programming cycles and gauge choices each instance has been annealed with (typically between 200 and 2000). Calculating a success probability p for each cycle, we compute the probability distribution of p over different cycles for each instance [21, 36]. We find that while for some instances p is essentially insensitive to programming errors, for other instances (even within the same thermal hardness group), p varies significantly, spanning several orders of magnitude. This is illustrated in Fig. 4 which presents some results based on a straightforward percentile analysis of these distributions. For instance #1 in the figure, the 80th percentile probability is $I_{q=0.8}(p) = 0.669(3)$, whereas the probability at the 90th percentile is $I_{q=0.9}(p) = 0.698(4)$. Hence the ratio $R_{8,9} = I_{q=0.8}(p)/I_{q=0.9}(p)$ is close to one. Conversely, for instance #35, the values are $I_{q=0.8}(p) = 0.008(1)$,

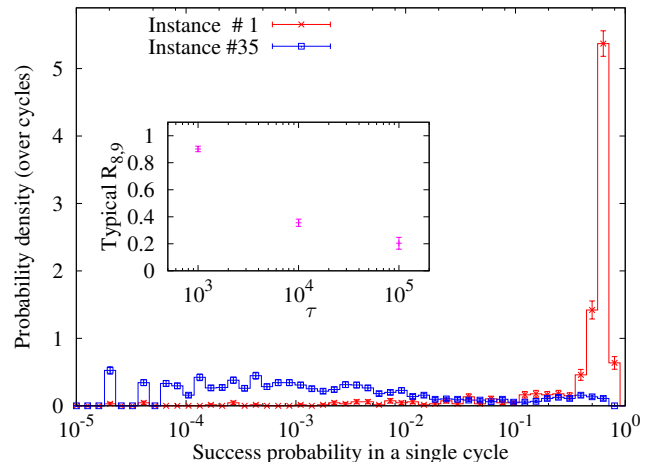


FIG. 4. **Empirical evidence for the absence/presence of ‘ J -chaos’.** Probability density of success probability of a single cycle, p , over different programming cycles. The probability densities are plotted here for two easy ($\tau = 10^3$) instances (here, $t_a = 20\mu\text{s}$ and the number of anneals per programming cycle is $X = 49500$, see Appendix A. Instance #1 (662 cycles) is typical in this τ -generation with success probability $p \sim 1$ in the majority of the programming cycles. On the other hand, instance #35 (1624 cycles) suffers from strong J -chaos: Even though the probability of finding $p \sim 0.1$ in some of the programming cycles is not negligible, most cycles are significantly less successful, e.g., the median p is $I_{q=0.5} = 6.7(5) \times 10^{-4}$. **Inset:** Typical ratio of the 80th percentile probability to the 90th percentile probability, namely $R_{8,9} = I_{q=0.8}/I_{q=0.9}$ (see text) as a function of τ (for $\tau \geq 10^6$ and 10^7 , $R_{8,9}$ was not computed due to extremely low success probabilities). Smaller ratios indicate larger fluctuations in success probabilities.

$I_{q=0.9}(p) = 0.07(2)$ and the ratio is $R_{8,9} = 0.12$, i.e., the success probability drops by an order of magnitude. The inset of Fig. 4 shows the typical ratio $R_{8,9}$ as a function of classical hardness, demonstrating the strong correlation between thermal hardness and the devastating effects of J -chaos caused by ICE, namely that the larger τ is, the more probable it is to find instances for which p varies wildly between programming cycles.

VI. DISCUSSION

We have devised a method for quantifying the ‘classicality’ of quantum annealers by studying their performance on sets of instances characterized by different degrees of thermal hardness, which we have defined for that purpose as the mixing (or equilibration) time τ of classical thermal algorithms (namely, PT) on these. We find that the 2D-like Chimera architecture used in the D-Wave chips does give rise to thermally very-hard, albeit rare, instances. Specifically, we have found samples that exhibit temperature chaos, and as such have very long mixing times, i.e., they are classically exceptionally hard

³ We refer to the *physical* temperature of the chip. However, non-equilibrium systems (e.g., supercooled liquids or glasses) can be characterized by *two* temperatures [44]: On the one hand, the physical temperature T which rules fast degrees of freedom that equilibrate. On the other hand, the ‘effective’ temperature refers to slow degrees of freedom that remain out of equilibrium. We are currently investigating whether or not the DW2 chip can analogously be characterized by two such temperatures.

to solve.

Applying our method to an experimental quantum annealing optimizer, the DW2 chip, we have found that its performance is more susceptible to changes in thermal hardness than classical algorithms. This is in contrast with the performance of the best-known state-of-the-art classical solver on Chimera graphs, the ‘non-thermal’ HFS algorithm, which scales (unsurprisingly) better. Our results are not meant to suggest that the DW2 chip is not a quantum annealer, but rather that its quantum properties may be significantly masked by much-undesired classical effects.

We have identified and quantified two probable causes for the observed behavior: A possibly too high temperature, or more probably, J -chaos, the random errors stemming from the digital-to-analog conversion in the programming of the coupling parameters. One may hope that the scaling of current DW2 chips would significantly improve if one or both of the above issues are resolved. Clearly, lowering the temperature of the chip and/or reducing the error involved in the programming of its parameters are both technologically very ambitious goals, in which case error correcting techniques may prove very useful [48]. We believe that quantum Monte Carlo simulations of the device will be instrumental in the understanding of the roles that temperature and magnitude of programming errors play in the performance of the chip (and of its classical counterparts). In turn, this will help sharpening the most pressing technological challenges facing the fabrication of these and other future quantum optimizing devices, paving the way to obtaining a long-awaited insights as to the difference between quantum and classical hardness in the context of optimization. We are currently pursuing these approaches.

ACKNOWLEDGMENTS

We thank Luis Antonio Fernández and David Yllanes for providing us with their analysis program for the PT correlation function. We also thank Marco Baity-Jesi for helping us to prepare the figures.

We are indebted to Mohammad Amin, Luis Antonio Fernández, Enzo Marinari, Denis Navarro, Giorgio Parisi, Federico Ricci-Tersenghi and Juan Jesús Ruiz-Lorenzo for discussions.

We thank Luis Antonio Fernández, Daniel Lidar, Felipe Llanes-Estrada, David Yllanes and Peter Young for their reading of a preliminary version of the manuscript.

We thank D-Wave Systems Inc. for granting us access to the chip.

We acknowledge the use of algorithms and source code for a classic solver, devised and written by Alex Selby, available for public usage at <https://github.com/alex1770/QUBO-Chimera>.

IH acknowledges support by ARO grant number W911NF-12-1-0523. VMM was supported by MINECO

(Spain) through research contract N° FIS2012-35719-C02.

Appendix A: Methods

Computation of the mixing time τ .— Because we follow Ref. [20], we just briefly summarize here the main steps of the procedure. Considering one of the N_T system copies in the PT simulation, let us denote the temperature of copy i at Monte Carlo time t by T_{i_t} , where $1 \leq i_t \leq N_T$ (see inset of Fig. 1). At equilibrium, the probability distribution for i_t is uniform (namely, $1/N_T$) hence the exact expectation value of i_t is $\langle i_t \rangle = (N_T + 1)/2$. From the general theory of Markov Chain Monte Carlo [18], it follows that the equilibrium time-correlation function may be written as a sum of exponentially decaying terms:

$$\begin{aligned} C_{PT}(s) &= \langle i_t i_{t+s} \rangle - \frac{(N_T + 1)^2}{4} \\ &= \sum_n a_n e^{-s/\tau_n} \quad (\tau_1 > \tau_2 > \dots). \end{aligned} \quad (A1)$$

The mixing time τ is the largest ‘eigen-time’ τ_1 . We compute numerically the correlation function $C_{PT}(s)$ and fit it to the decay of *two* exponential functions (so we extract the dominant time scale τ and a sub-leading time scale). The procedure is described in full in Ref. [20].

D-wave data acquisition and analysis.—

Data acquisition:

In what follows we briefly summarize the steps of the experimental setup and data acquisition for the anneals performed on the 414 randomly-generated instances in the various thermal-hardness groups.

1. The J_{ij} couplings of each of the 414 instances have been encoded onto the D-Wave chip using many different choices of annealing times in the allowed range of $20\mu s \leq t_a \leq 20ms$.
2. For each instance and each choice of t_a the following process has been repeated hundreds to thousands of times:

- (a) First, a random ‘gauge’ has been chosen for the instance. A gauge transformation does not change the properties of the optimization problem but has some effect on the performance of the chip which follows from the imperfections of the device that break the gauge symmetry. The different gauges are applied by transforming the original instance $h_i \rightarrow \eta_i h_i$, $J_{ij} \rightarrow \eta_i \eta_j J_{ij}$, to the original cost function Eq. (1). The above gauge transformations correspond to the change $s_i \rightarrow \eta_i s_i$ in configuration spin values. Here, the N gauge parameters $\eta_i = \pm 1$ were chosen randomly.

- (b) The chip was then programmed with the gauge-transformed instance (inevitably adding programming bias errors, as mentioned in the main text).
- (c) The instance was then solved, or annealed, X times within the programming cycle/with the chosen gauge. We chose $X \approx 1\text{sec}/t_a$, the maximally allowed amount.
- (d) After the X anneals were performed, the number of successes Y , i.e., the number of times a minimizing configuration had been found, was recorded. The probability of success for the instance, for that particular gauge/programming cycle and annealing time t_a was then estimated as $p = Y/X$. Note, that in cases where the probability of success is of the order of $1/X$, the probability p will be a rather noisy estimate (see data analysis, below, for a procedure to mitigate this problem).
- (e) If the prefixed number of cycles for the current instance and t_a has not been reached, return to (2a) and choose a new gauge.

Data analysis and time-to-solution estimates:

The analysis of the data acquisition process described above proceeded as follows.

1. For each instance and each annealing time, the total number of hits $Y_{\text{tot}} = \sum_i Y_i$ was calculated, where i sums over all the gauge/programming cycles. Denoting $X_{\text{tot}} = \sum_i X_i$ as the total number of annealing attempts, the probability of success for any particular instance and anneal time was then calculated as $P = Y_{\text{tot}}/X_{\text{tot}}$.
2. The above probability was then converted into an average time-to-solution t_s for that instance and t_a according to $t_s = t_a/P$, where the special case of $P = 0$ designates an estimate of an infinite t_s , where in practice the true probability lies below the resolution threshold of $1/X_{\text{tot}}$.
3. A typical runtime for a hardness group was then obtained by taking the median over all minimal t_s values of all the instances in the group.

Appendix B: Instance generation and analysis

1. The Parallel Tempering simulations

We briefly outline the technical details of the Parallel Tempering (PT) simulations and subsequent analysis performed on the randomly generated instances. The reader is referred to Ref. [20] for further details.

To run the simulations, we employed multi-spin coding [49], a simple yet efficient form of parallel computation, that allows the simultaneous simulations of a large number of problem instances. The name *multi-spin* follows from the fact that our dynamic variables are binary, $s_i = \pm 1$, and thus can be coded in a single bit. Hence, one may code the i -th spin corresponding to M independent instances in a single M -bit computer word. Using streaming extensions, M can be as large as $M = 256$, nowadays.⁴ The advantages of simulating in parallel 256 instances are obvious, if we want to study a *huge* number of problems in our quest for these rare instances displaying Temperature Chaos. In fact, we have simulated a total of $N_S = 303 \times 256 = 77568$ problem instances.

The temperature grid of the PT simulations consisted of $N_T = 30$ temperatures. Temperatures with indices $i = 13, 14, \dots, N_T$ were evenly distributed in the range $0.21 \leq T_i \leq T_{\text{max}} = 1.632$, while lower temperatures in the range $T_{\text{min}} = 0.045 \leq T_i \leq 0.2$ (indices $i = 1, 2, \dots, 12$) have been added in order to detect temperature chaos effects.⁵ Ergodicity was maintained by the temperature-swap part of the PT.

For each instance, we ran four independent simulations (i.e., four replicas) per temperature, where an elementary Monte Carlo step consisted of 10 full lattice Metropolis sweeps, followed by a PT temperature swap attempt. Since the Chimera lattice is bipartite, Metropolis sweeps have been carried out on alternating partitions at each step.

The calculation of the mixing time τ was conducted in three stages, or rounds (see also Ref. [20]). In the first stage, all 303×256 instances were simulated for a total of 10^6 elementary Monte Carlo steps (i.e., each system was simulated for 10^7 full-lattice Metropolis sweep). At the end of each round the mixing time τ was computed (measured in units of full-lattice Metropolis sweeps). As can also be read off Fig. 1 of the main text, the first-round of simulations was adequate for the equilibration of most instances, namely, for problems of τ -generations 10^3 , 10^4 and 10^5 . The second round of simulations was set to last 10 times longer, consisting of 10^7 elementary Monte Carlo steps, or 10^8 full-lattice Metropolis sweeps per system. These longer simulations were reserved only to the 1024 hardest instances corresponding to τ -generations of 10^6 or larger.⁶ The 256 worse-scoring instances of these

⁴ Simulations were run on a standard Intel(R) Xeon(R) processors (E5-2690 0 @ 2.90GHz).

⁵ In our simulations, the minimal temperature value $T_{\text{min}} = 0.045$ corresponds effectively to zero temperature. This follows from the minimal energy gap of our instances being $\Delta = 2$ together with our use of a 64-bit (pseudo) random-number generator [50]. Setting T_{min} such that it obeys $2^{64} \times e^{-2/T_{\text{min}}} < 1$, our Metropolis simulations at T_{min} effectively become equivalent to $T = 0$ simulations.

⁶ The criterion for selecting the hardest instances to qualify for subsequent rounds of simulations was done by assigning a figure of merit for each instance based on the performance of its $4 \times$

were further simulated for 10^8 elementary Monte Carlo steps (or 10^9 full-lattice Metropolis sweeps per system). This simulation lasted 10 days on our fastest CPU [Intel(R) Core(TM) i7-4770K CPU @ 3.50GHz]. From it, we obtained 14 extremely hard problem instances, belonging to τ -generation 10^7 .

2. Spin-overlap analysis

Here, we briefly extend the analysis of the energy landscapes of thermally-hard problems, initiated in Fig. 2 of the main text. To do so, we make use of the notion of ‘spin-overlap’, which plays a major role in any spin glass investigation (see, e.g., Ref. [11]). The spin overlap q between two N -spin configurations $\{s_i^a\}$ and $\{s_i^b\}$ is defined as

$$q = 1 - 2 \frac{N_{a,b}}{N}, \quad (\text{B1})$$

where $N_{a,b}$ is the Hamming distance between the two configurations, i.e., the number of spins by which the two configurations *differ*. For two identical configurations we get $N_{a,b} = 0$ and $q = 1$ while for two configurations differing by a global spin flip (i.e., $s_i^a = -s_i^b$ for all i) we have $N_{a,b} = N$ and $q = -1$. Since the instances we study all have $h_i = 0$, their Hamiltonians possess a global bit-flip symmetry. For any configuration $\{s_i^a\}$, its spin-reversed configuration $\{s_i^b\} = -\{s_i^a\}$ has the same energy. We have therefore chosen to consider the more informative measure of the absolute value of the overlap, $|q|$. In this case, the maximum meaningful Hamming distance between any two configurations is $N/2$.

We utilized spin overlaps to investigate the energy landscapes of the various instances in the following way. During the PT simulations, 12000 spin configurations of each instance were stored on disk, corresponding to 100 evenly spaced check-points in Monte Carlo time where every check-point contains $4 \times 30 = 120$ configurations. Of those, ground-state (GS) configurations⁷ and minimally-excited (ES) states were picked out for further analysis. Our analysis consisted of examining the probability distributions of overlaps between (i) randomly chosen GS configurations and randomly chosen ES configurations [GS-ES, solid blue curves in Fig. 5 of Extended Data (ED)] and (ii) pairs of randomly chosen GS configurations (GS-GS, dashed red curves in Fig. 5). Two extremal cases were encountered. For easy instances

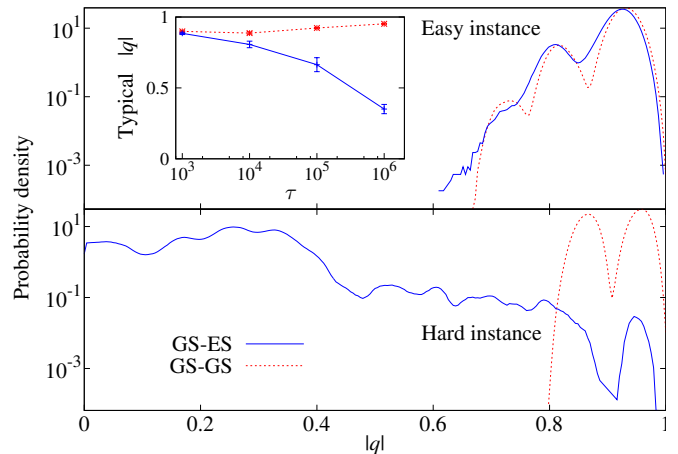


FIG. 5. Probability distribution of the spin overlap $|q|$ between ground states and minimally excited states (GS-ES, solid blue curves). For comparison, we also show the overlap between different ground states (GS-GS, dashed red curves). The distributions shown were computed for the same instances considered in Fig. 2 of main text, with mixing time generations $\tau \approx 10^3$ (top) and $\tau \approx 10^6$ (bottom). **Inset: Dependence of the overlap between ground states and minimally excited states on τ .** Typical median GS-ES overlap $|q|$ averaged over each hardness group as a function of τ -generation (blue points, the lines are to guide the eye). The red points are GS-GS typical overlaps shown for comparison.

(Fig. 5–top), the probability density for GS-GS overlaps is very similar to the probability density for GS-ES overlaps. This is expected in cases where ES states are trivially connected to GS states via one spin-flip. Conversely, for hard instances (Fig. 5–bottom), the probability densities for GS-GS overlaps and for GS-ES overlaps differ significantly, indicating that the vast majority of the ES states encountered during the simulations are not trivially connected to typical GS configurations but are rather very distant from them.

The top and bottom panels of Fig. 5 describe only two representative instances, however the above depiction was also found to be valid in the general case, as is confirmed by calculation of the typical $|q|$ for all the instances in each of the hardness groups.⁸ As the inset of Fig. 5 shows, the harder instances are, the further away minimally excited states are from ground states.

⁷ $30 = 120$ system copies. For each of the copies, the fraction of Monte Carlo time spent at the higher-temperatures regions, namely T_i with $i = 16, 17, \dots, N_T$, was calculated where the figure of merit was chosen to be the smallest of these fractions, which was used as an indication for how trapped the instance is in the low-temperatures region.

⁸ For a $J = \pm 1$ spin-glass, the ground state is typically highly degenerate even in two dimensions [51]. Empirically, we find that this high-degeneracy is also present on the 2D-like Chimera [38].

⁸ In order to define a typical $|q|$, we follow a two-steps procedure. First, we obtain a typical $|q|$ for each instance by computing the median overlap [e.g. for the easy instance in the top panel of Fig. 5 $\text{med}(|q|) = 0.918$, while for the hard instance in the bottom panel $\text{med}(|q|) = 0.25$]. Second, we average over all the instances in a τ -generation, by computing the median over the instance medians.

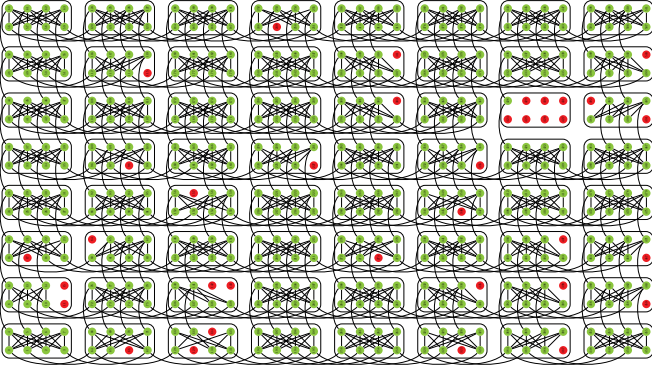


FIG. 6. The 476-qubit DW2 device architecture and qubit connectivity.

Appendix C: The D-Wave Two Chip

1. The Chimera

The Chimera graph of the D-Wave Two (DW2) chip used in this study is shown in Fig. 6. The chip is an 8×8 array of unit cells where each unit cell is a balanced $K_{4,4}$ bipartite graph of superconducting flux qubits. In the ideal Chimera graph the degree of each (internal) vertex is 6. On our chip, only a subset of 476 qubits, is functional. The temperature of the device $\sim 15\text{mK}$.

The chip is designed to solve a very specific type of problems, namely, Ising-type optimization problems where the cost function is that of the Ising Hamiltonian [see Eq. (1) of the main text]. The Ising spins, $s_i = \pm 1$ are the variables to be optimized over and the sets $\{J_{ij}\}$ and $\{h_i\}$ are the programmable parameters of the cost function. In addition, $\langle ij \rangle$ denotes a sum over all active edges of the Chimera graph.

2. The D-Wave Two annealing schedule

The DW2 performs the annealing by implementing the time-dependent Hamiltonian

$$H(t) = -A(t) \sum_i \sigma_i^x + B(t) H_{\text{Ising}}, \quad (\text{C1})$$

with $t \in [0, t_a]$ where the allowed range of annealing times t_a , due to engineering restrictions, is between $20\mu\text{s}$ and 20ms . The annealing schedules $A(t)$ and $B(t)$ used in the device are shown in Fig. 7. There are four annealing lines, and their synchronization becomes harder for faster annealers. The filtering of the input control lines introduces some additional distortion in the annealing control.

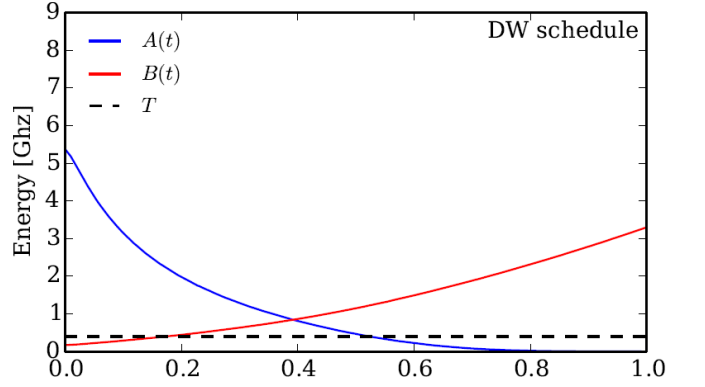


FIG. 7. Annealing schedule of the D-Wave chip. The functions $A(t)$ and $B(t)$ are the amplitudes of the (transverse-field) driver and classical Ising Hamiltonians, respectively. Also shown is the temperature in units of energy ($k_B = 1$).

3. Gauge averaging on the D-Wave device

Calibration inaccuracies stemming mainly from the digital to analog conversions of the problem parameters, cause the couplings J_{ij} and h_i realized on the DW2 chip to be slightly different from the intended programmed values (with a typical $\sim 5\%$ variation). Therefore, instances encoded on the device will be generally different from the intended instances. Additionally, other, more systematic biases exist which cause spins to prefer one orientation over another regardless of the encoded parameters. To neutralize these effects, it is advantageous to perform multiple annealing rounds (or ‘programming cycles’) on the device, where each such cycle corresponds to a different encoding or ‘gauge’ of the same problem instance onto the couplers of the device [9]. To realize these different encodings, we use a gauge freedom in realizing the Ising spin glass: for each qubit we can freely define which of the two qubits states corresponds to $s_i = +1$ and $s_i = -1$. More formally this corresponds to a gauge transformation that changes spins $s_i \rightarrow \eta_i s_i$, with $\eta_i = \pm 1$ and the couplings as $J_{ij} \rightarrow \eta_i \eta_j J_{ij}$ and $h_i \rightarrow \eta_i h_i$. The simulations are invariant under such a gauge transformation, but due to calibration errors which break the gauge symmetry, the results returned by the DW2 are not.

4. Performance of the DW2 chip as a function of annealing time

Since the DW2 chip is a putative quantum annealer, it is only natural to ask how its performance, namely, the typical time-to-solution t_s it yields, depends on annealing time t_a . Ideally, the longer t_a is, the better the performance we expect [52]. However, in practice, decohering interactions with the environment are present which be-

come more pronounced with longer running times of the annealing process. It is therefore plausible to assume that there is an optimal t_a for which t_s is shortest [9].

Analysis of the dependence of success probabilities, or equivalently times to solution, on annealing time is found to be heavily blurred, or masked, by fluctuations in the success probability between different programming cycles. These fluctuations, which become more pronounced for harder instances, stem from the noisy encoding of the instance parameters already discussed above. Any meaningful analysis of the dependence of success probability on annealing time must therefore successfully average out these effects therefore requires many rounds of anneals. Unfortunately (see data acquisition in Appendix A) the number of annealing attempts X for a given DW2 programming cycle is proportional to $1/t_a$, ranging from $X^{t_a=20\mu s} = 49500$, to $X^{t_a=20ms} = 49$. As a consequence, the minimal success probability that can be measured from a $t_a = 20ms$ programming cycle is just $p_{\min}^{20ms} = 1/49 \approx 0.02$. While this limitation is not serious for easy instances (i.e., those of the $\tau = 10^3$ group), for hard instances a typical success probability p is much smaller than 0.02. This problem can be alleviated by running the DW2 chip on the same instance (and t_a) multiple number of times (with a different gauge for each cycle, but with t_a held fixed), and then averaging the resulting p over programming cycles. In this way, the minimal success probability that can be measured is $1/(XN_{\text{cycles}})$. For N_{cycles} in the hundreds typically, typical numbers for the minimal measurable success probability were

$$p_{\min}^{20\mu s} \approx 6.5 \times 10^{-8}, \quad p_{\min}^{200\mu s} \approx 3.3 \times 10^{-6}, \\ p_{\min}^{2ms} \approx 4 \times 10^{-5} \quad \text{and} \quad p_{\min}^{20ms} \approx 5.1 \times 10^{-4}.$$

However, we have found that the above minimal-probability thresholds are still too high for our hardest problems, $\tau \geq 10^6$. To overcome this problem, we groups the success probabilities into annealing-time windows: $20\mu s \leq t_a/10^k < 60\mu s$ and $60\mu s \leq t_a/10^k < 200\mu s$ for $k = 0, 1, 2$ (where in the largest-time interval, $k = 2$ above, we also included the $t_a = 20ms$ data).

At this point, the success probability needs to be averaged over the problem instances of a given τ -generation. Given the extreme problem-to-problem fluctuations, percentiles have been calculated. In Fig. 8–top we show the 50th percentile (i.e., the median) as a function of probability. Unfortunately, in spite of our efforts to increase the experimental sensitivity, the measured success probability yielded zero for more than a half of the instances with $\tau = 10^5$ and $\tau = 10^6$. Hence, we show Fig. 8–bottom the results for the 80th percentile.

In all cases, we found that a power law description

$$p(\tau, t_a) \sim t_a^{\theta(\tau)}, \quad (C2)$$

is adequate, although the exponent θ depends significantly both on τ and on the percentile considered (see Fig 9). The trends are very clear. For easy instances, p barely depends on t_a (yielding $\theta \approx 0$). In fact, the exponent θ increases with increasing τ , meaning that the

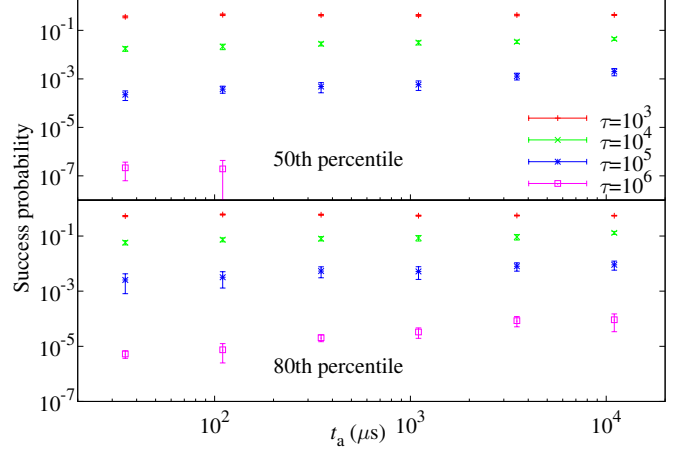


FIG. 8. **Dependence of success probability on annealing time.** Typical success probability (see main text for details) as a function of annealing time for the various hardness groups. Shown are the 50th and 80th percentiles within each hardness group (top and bottom panels, respectively).

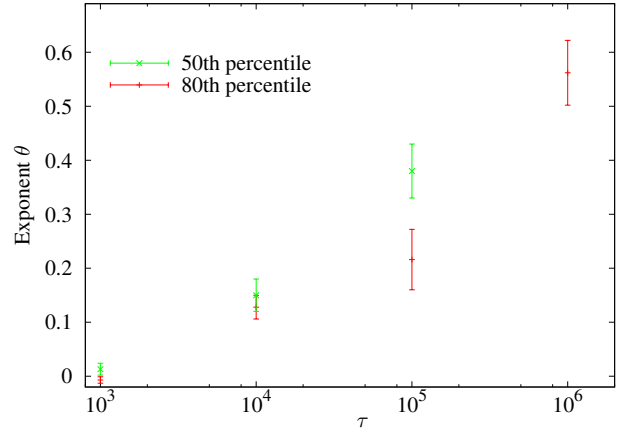


FIG. 9. **Dependence of success probability on annealing time.** The exponent θ of Eq. (C2), as computed from the data shown in Fig. 8, plotted against τ -generation.

harder the instance is, the more it typically benefits from increasing t_a .

Recalling that time to solution is given by $t_s = t_a/p \sim t_a^{1-\theta}$, we find that the exponent θ in Eq. (C2) is less than 1 for all hardness groups, i.e., that the shorter the annealing time is, the shorter the time-to-solution becomes. Since however this trend can not hold all the way down to $t_a = 0$, these results therefore imply that there exist for each group an optimal annealing time that is however below the shortest-accessible $t_a = 20\mu s$. Furthermore, the increase of θ with hardness group can be interpreted as the harder the instances are, the longer the typical optimal annealing time is, consistently with what

one would expect from a quantum annealer. It is important to note at this point that the highly-fluctuating success probability, stemming from programming errors,

unfortunately does not allow for a more sensitive analysis and that more robust results could be obtained if the programming errors leading to J -chaos were to be reduced.

-
- [1] P. W. Shor, in *Proc. 35th Symp. on Foundations of Computer Science*, edited by S. Goldwasser (1994) p. 124.
 - [2] L. K. Grover, *Phys. Rev. Lett.* **79**, 325 (1997).
 - [3] M. Schlosshauer, *Rev. Mod. Phys.* **76**, 1267 (2004).
 - [4] M. W. Johnson *et al.*, *Nature* **473**, 194 (2011).
 - [5] T. Albash, S. Boixo, D. A. Lidar, and P. Zanardi, *New Journal of Physics* **14**, 123016 (2012).
 - [6] T. Lanting, A. J. Przybysz, A. Y. Smirnov, F. M. Spedalieri, M. H. Amin, A. J. Berkley, R. Harris, F. Altomare, S. Boixo, P. Bunyk, N. Dickson, C. Enderud, J. P. Hilton, E. Hoskinson, M. W. Johnson, E. Ladizinsky, N. Ladizinsky, R. Neufeld, T. Oh, I. Perminov, C. Rich, M. C. Thom, E. Tolkacheva, S. Uchaikin, A. B. Wilson, and G. Rose, *Phys. Rev. X* **4**, 021041 (2014).
 - [7] J. A. Smolin and G. Smith, “Classical signature of quantum annealing,” *ArXiv:1305.4904*.
 - [8] S. W. Shin, G. Smith, J. A. Smolin, and U. Vazirani, *arXiv:1401.7087* (2014).
 - [9] T. F. Ronnow, Z. Wang, J. Job, S. Boixo, S. V. Isakov, D. Wecker, J. M. Martinis, D. A. Lidar, and M. Troyer, *Science* **345**, 420 (2014).
 - [10] S. Boixo, T. F. Ronnow, S. V. Isakov, Z. Wang, D. Wecker, D. A. Lidar, J. M. Martinis, and M. Troyer, *Nat Phys* **10**, 218 (2014).
 - [11] A. P. Young, ed., *Spin Glasses and Random Fields* (World Scientific, Singapore, 1998).
 - [12] F. Belletti, M. Cotallo, A. Cruz, L. A. Fernandez, A. Gordillo, A. Maiorano, F. Mantovani, E. Marinari, V. Martin-Mayor, A. Muñoz Sudupe, D. Navarro, S. Perez-Gaviro, J. J. Ruiz-Lorenzo, S. F. Schifano, D. Sciretti, A. Tarancon, R. Tripiccion, and J. L. Velasco (Janus Collaboration), *Comp. Phys. Comm.* **178**, 208 (2008), *arXiv:0704.3573*.
 - [13] F. Belletti, M. Guidetti, A. Maiorano, F. Mantovani, S. F. Schifano, R. Tripiccion, M. Cotallo, S. Perez-Gaviro, D. Sciretti, J. L. Velasco, A. Cruz, D. Navarro, A. Tarancon, L. A. Fernandez, V. Martin-Mayor, A. Muñoz-Sudupe, D. Yllanes, A. Gordillo-Guerrero, J. J. Ruiz-Lorenzo, E. Marinari, G. Parisi, M. Rossi, and G. Zanier (Janus Collaboration), *Computing in Science and Engineering* **11**, 48 (2009).
 - [14] M. Baity-Jesi, R. A. Baños, A. Cruz, L. A. Fernandez, J. M. Gil-Narvion, A. Gordillo-Guerrero, D. Iniguez, A. Maiorano, F. Mantovani, E. Marinari, V. Martin-Mayor, J. Monforte-Garcia, A. Muñoz Sudupe, D. Navarro, G. Parisi, S. Perez-Gaviro, M. Pivanti, F. Ricci-Tersenghi, J. J. Ruiz-Lorenzo, S. F. Schifano, B. Seoane, A. Tarancon, R. Tripiccion, and D. Yllanes (Janus Collaboration), *Comp. Phys. Comm* **185**, 550 (2014), *arXiv:1310.1032*.
 - [15] K. Hukushima and K. Nemoto, *J. Phys. Soc. Japan* **65**, 1604 (1996), *arXiv:cond-mat/9512035*.
 - [16] E. Marinari, in *Advances in Computer Simulation*, edited by J. Kertész and I. Kondor (Springer-Verlag, 1998) p. 50, (*arXiv:cond-mat/9612010*).
 - [17] S. Kirkpatrick, C. D. Gelatt, Jr., and M. P. Vecchi, *Science* **220**, 671 (1983).
 - [18] A. Sokal, in *Functional Integration: Basics and Applications*, edited by C. DeWitt-Morette, P. Cartier, and A. Folacci (Plenum, 1997).
 - [19] L. A. Fernandez, V. Martin-Mayor, S. Perez-Gaviro, A. Tarancon, and A. P. Young, *Phys. Rev. B* **80**, 024422 (2009).
 - [20] R. Alvarez Baños, A. Cruz, L. A. Fernandez, J. M. Gil-Narvion, A. Gordillo-Guerrero, M. Guidetti, A. Maiorano, F. Mantovani, E. Marinari, V. Martin-Mayor, J. Monforte-Garcia, A. Muñoz Sudupe, D. Navarro, G. Parisi, S. Perez-Gaviro, J. J. Ruiz-Lorenzo, S. F. Schifano, B. Seoane, A. Tarancon, R. Tripiccion, and D. Yllanes (Janus Collaboration), *J. Stat. Mech.* **2010**, P06026 (2010), *arXiv:1003.2569*.
 - [21] L. A. Fernandez, V. Martin-Mayor, G. Parisi, and B. Seoane, *EPL* **103**, 67003 (2013), *arXiv:1307.2361*.
 - [22] S. R. McKay, A. N. Berker, and S. Kirkpatrick, *Phys. Rev. Lett.* **48**, 767 (1982).
 - [23] A. J. Bray and M. A. Moore, *Phys. Rev. Lett.* **58**, 57 (1987).
 - [24] J. R. Banavar and A. J. Bray, *Phys. Rev. B* **35**, 8888 (1987).
 - [25] I. Kondor, *J. Phys. A* **22**, L163 (1989).
 - [26] I. Kondor and Végő, *J. Phys. A* **26**, L641 (1993).
 - [27] A. Billoire and E. Marinari, *J. Phys. A* **33**, L265 (2000).
 - [28] T. Rizzo, *J. Phys.* **34**, 5531 (2001).
 - [29] R. Mulet, A. Pagnani, and G. Parisi, *Phys. Rev. B* **63**, 184438 (2001).
 - [30] A. Billoire and E. Marinari, *Europhys. Lett.* **60**, 775 (2002).
 - [31] F. Krzakala and O. C. Martin, *Eur. Phys. J.* **28**, 199 (2002).
 - [32] T. Rizzo and A. Crisanti, *Phys. Rev. Lett.* **90**, 137201 (2003).
 - [33] G. Parisi and T. Rizzo, *J. Phys. A* **43**, 235003 (2010).
 - [34] M. Sasaki, K. Hukushima, H. Yoshino, and H. Takayama, *Phys. Rev. Lett.* **95**, 267203 (2005).
 - [35] H. G. Katzgraber and F. Krzakala, *Phys. Rev. Lett.* **98**, 017201 (2007).
 - [36] A. Billoire, *J. Stat. Mech.* **2014**, P04016 (2014), *arXiv:1401.4341*.
 - [37] C. K. Thomas, D. A. Huse, and A. A. Middleton, *Phys. Rev. Lett.* **107**, 047203 (2011), *arXiv:1103.1946*.
 - [38] H. G. Katzgraber, F. Hamze, and R. S. Andrist, *Phys. Rev. X* **4**, 021008 (2014).
 - [39] F. Hamze and N. de Freitas, in *Proceedings of the 20th Conference on Uncertainty in Artificial Intelligence*, UAI '04 (AUAI Press, Arlington, Virginia, United States, 2004) pp. 243–250.
 - [40] A. Selby, “Efficient subgraph-based sampling of Ising-type models with frustration,” (2014), *arXiv:1409.3934*.
 - [41] I. Hen and A. P. Young, *Phys. Rev. E* **84**, 061152 (2011), *arXiv:1109.6872v2*.
 - [42] E. Farhi, D. Gosset, I. Hen, A. W. Sandvik, P. Shor, A. P. Young, and F. Zamponi, *Phys. Rev. A* **86**, 052334

- (2012), (arXiv:1208.3757).
- [43] Jamie King, Private Communication (2014).
 - [44] L. F. Cugliandolo, J. Kurchan, and L. Peliti, Phys. Rev. E **55**, 3898 (1997).
 - [45] M. Nifle and H. J. Hilhorst, Phys. Rev. Lett. **68**, 2992 (1992).
 - [46] M. Ney-Nifle, Phys. Rev. B **57**, 492 (1998).
 - [47] F. Krzakala and J. P. Bouchaud, Europhys. Lett. **72**, 472 (2005).
 - [48] K. L. Pudenz, T. Albash, and D. A. Lidar, Nature Communications **5**, 3243 (2014).
 - [49] M. E. J. Newman and G. T. Barkema, *Monte Carlo Methods in Statistical Physics* (Oxford University Press Inc., New York, USA, 1999).
 - [50] L. A. Fernandez, V. Martin-Mayor, and D. Yllanes, Nucl. Phys. B **807**, 424 (2009).
 - [51] F. Barahona, T. Maynard, R. Rammal, and J. P. Uhry, J. Phys. A **15**, 673 (1982).
 - [52] T. Kadowaki and H. Nishimori, Phys. Rev. E **58**, 5355 (1998).